



PCCP

Achieving tunable chemical reactivity through photo initiation of energetic materials at metal oxide surfaces

Journal:	<i>Physical Chemistry Chemical Physics</i>
Manuscript ID	CP-ART-07-2020-004069.R1
Article Type:	Paper
Date Submitted by the Author:	26-Sep-2020
Complete List of Authors:	Kuklja, Maija; University of Maryland at College Park, Mater.Sci.Eng.; National Science Foundation, Office of the Director Tsyshevsky, Roman; University of Maryland at College Park, Materials Science and Engineering Zverev, Anthon; Institute of Coal Chemistry and Material Science SB RAS Mitrofanov, Anatoly; Kemerovo State University, Solid State Chemistry and Meterials Research Ilyakova, Natalya; Kemerovo State University Nurmukhametov, Denis; Institute of Coal Chemistry and Material Science SB RAS Rashkeev, Sergey N. ; University of Maryland at College Park, Materials Science and Engineering

SCHOLARONE™
Manuscripts

Achieving tunable chemical reactivity through photo initiation of energetic materials at metal oxide surfaces

Maija M. Kuklja^{1,*}, Roman Tsyshevsky¹, Anton S. Zverev^{2,3}, Anatoly Mitrofanov³, Natalya Ilyakova³, Denis R. Nurmukhametov², and Sergey N. Rashkeev¹

¹ *Department of Materials Science and Engineering, University of Maryland, College Park, MD 20742, USA*

² *Institute of Coal Chemistry and Chemical Materials Science, Siberian Branch, Russian Academy of Sciences, Kemerovo, Russia*

³ *Kemerovo State University, Kemerovo, Russia*

Abstract

Known applications of high energy density materials are impressively vast. Despite this, we argue that energetic materials are still underutilized for common energy purposes due to our inability to control explosive chemical reactions releasing energy from these materials. The situation appears paradoxical as Energetic Materials (EM) possess massive amounts of energy and, hence, should be most appropriate for applications in many energy-intensive processes. Here, we discover how chemical decomposition reactions can be stimulated with laser excitation and therefore, highly controlled by selectively designing energetic material – metal oxide interfaces with an example of Pentaerythritol Tetranitrate (PETN)-MgO and Trinitrotoluene (TNT)-MgO composite samples. Our density functional theory and embedded cluster method calculations were combined with measurements of the optical absorption spectra and laser initiation experiments. We found that first (1064 nm, 1.17 eV), second (532, 2.33 eV), and third (355 nm, 3.49 eV) laser harmonics, to all of which pure energetic materials are transparent, can be effectively used to trigger explosive reactions in the PETN-MgO samples. We propose a consistent electronic mechanism that explains how specific sub-band optical transitions initiate decomposition chemistry. Also, this selectivity reveals a fundamental difference between materials chemistry at interfaces as we show on examples of PETN and TNT energetic materials.

Key words: sub-band excitation, laser initiation of decomposition chemistry, high energy density materials, organic-inorganic interfaces

* Corresponding author, mkukla@nsf.gov with cc mkukla@umd.edu

1 Introduction

Energetic materials, storing high amount of chemical energy, are a wide class of materials that has been known and used for centuries¹. With a stunningly broad set of vast applications of energetic materials, ranging from high explosives to rocket fuels, from fireworks to railroad construction devices, and from pyrotechnics to medications¹, the potential of these materials is underutilized as the release of energy is difficult to control. High explosives are reactive energetic materials that can release energy very rapidly upon an external perturbation and thus producing an explosion, which is usually accompanied by light, heat, sound, and pressure. Examples of explosives include nitroglycerin, acetone peroxide, TNT (2-methyl-1,3,5-trinitrobenzene, also known as trinitrotoluene, $C_7H_5N_3O_6$), cellulose nitrate, RDX (1,3,5-Trinitroperhydro-1,3,5-triazine, $C_3H_6N_6O_6$), PETN (Pentaerythritol tetranitrate, $C_5H_8N_4O_{12}$), HMX (1,3,5,7-Tetranitro-1,3,5,7-tetrazocane, $C_4H_8N_8O_8$), etc.². Interestingly, the same energetic materials are used as both high explosives and medications. In medicine, nitroglycerin corrects the imbalance between the flow of oxygen and blood to the heart which removes painful symptoms of ischemic heart disease^{3,4}. Some other nitrates, e.g., PETN, are also used in medicine for the treatment of heart conditions^{5,6}. These drugs work by releasing the signaling gas nitric oxide in the body⁷.

Energetic high explosive materials are characterized by their sensitivity (an ability to initiate an explosive reaction upon an external stimulus – the less sensitive is the material, the better - as the more stable material is safer to use) and performance (a measure of destructive power due to the reaction propagation after ignition – the higher performance, the better – as the higher heat and higher detonation pressure is produced in the detonation wave)^{8,9}. Typically, the explosive reaction proceeds fast, producing a lot of heat, so the energy does not have a chance to dissipate. In addition

to a violent release of energy, chemical explosions must provide a means to transfer the energy into mechanical work^{10,11}. This is accomplished by expanding product gases from the reaction. Unfortunately, the high energy released in these explosions is uncontrollable and hence largely lost. Paradoxically, our inability to control chemical explosion reactions releasing the energy in desired quantities leads to the lack of effective technologies to use high energy density materials (that are supposed to be most appropriate) for energy applications. An illustrative analogy comes to mind. The relation between an explosion and such a controlled chemical reaction would be similar to the relation between a nuclear bomb (where massive destructive power is coming from uncontrolled fission reactions) and a nuclear reactor (where nuclear chain reactions are controlled and contained), which generates electric and heat energy¹². In particular, there were attempts to use energetic materials¹³ and waste energetic materials¹⁴ produced during the manufacture of explosives energetic materials for combustion in an industrial boiler, which is a compelling alternative disposal option for EM. In this process, the energy is captured from the fuel. Also, this technology would mitigate many environmental hazards. Another systematic investigation of the effect of micro- and nanoscale energetic materials in formulations of aluminum microparticles (Al MPs; heat source)/aluminum nanoparticles (Al NPs; heat source)/copper oxide nanoparticles (CuO NPs; oxidizer) on the combustion and gas-generating properties of sodium azide microparticles (NaN₃ MPs; gas-generating agent) for potential applications in gas generators was recently performed¹⁵.

To gain a reliable control over the reactions in energetic materials, it is critical to establish fundamental physical and chemical micro-mechanisms of their decomposition. Despite impressive recent advances in the field², this knowledge is still fragmentary and incremental, and it needs to be systematized. In particular, it is well-known that the sensitivity of an energetic material could significantly change when this material is mixed up with another material. This means that an

explosive reaction could be modified by the presence of interfaces. Certainly, the type of the interface also plays an important role. Such a phenomenon is similar to what one observes in heterogeneous catalysis where the chemical reactions could be controlled by interfaces¹⁶. Also, a selective bond breaking in energetic materials should occur at the presence of electromagnetic irradiation of certain wavelength, which is analogous to photocatalytic reactions¹⁷. For this purpose, one could use various laser irradiation methodologies that are widely used in studies of catalysis and photocatalysis¹⁸.

The laser irradiation is promising for selective, predictive, and controlled initiation of the energy release in energetic materials. However, unlike photochemistry of biomolecules¹⁹ or gas molecules^{20,21}, which is now a relatively well-established field, light-induced chemistry of surfaces or organic-inorganic interfaces involving energetic molecules is a rapidly emerging area of research with many unresolved questions^{22,23,24,25,26,27}. Although the possibility of photolysis of energetic materials has been long realized^{28,29}, a useful method has only recently been developed^{30,31} because most energetic materials are transparent to visible light and cannot be decomposed directly, but only by radiation with wavelengths shorter than 190 nm^{32,33}. An understanding of individual photoinduced processes in relation to specific interface structures³⁴ and the knowledge of mechanisms of energy accumulation and release³⁵ remain among outstanding challenges that hamper advances in new technologies and novel applications of engineered interfaces.

To explore whether the photo-stimulated chemical reactivity of high energy density materials can be controlled and tuned, (that is engineered and manipulated)^{36,37}, we have recently demonstrated that the electronic structure and optical properties of PETN molecule adsorbed on MgO and α -Al₂O₃ surfaces significantly differ from the properties of individual components (the molecule and the oxide surface)^{38,39}. We performed first principles calculations of a prototype organic-inorganic interface between a nitroester (PETN) and an oxide surface (magnesium oxide (MgO)³⁸ and aluminum oxide

(α -Al₂O₃)³⁹). Our study suggested that the light absorption is defined by the band alignment between interface components and interfacial charge transfer coupled with electronic states in the band gap, generated by oxide surface defects. The obtained results^{38,39} offer a coherent interpretation of experiments on selective laser initiation of energetic materials^{30,31}, which reported that the presence of metal oxide additives triggered the photoinitiation by an excitation energy much lower than the fundamental band gap. We proposed that PETN photodecomposition at the oxide interface is catalyzed by oxygen vacancies (F⁰ centers) at the MgO surface³⁸ and Al₂O₃ surface³⁹.

In this research, aimed at expanding, validating, and refining theoretical findings from our previous investigations, we performed a joint theoretical and experimental study on optical absorption and laser initiation of composite materials prepared by mixing well-studied and widely used high energy density materials PETN (Figure 1a) and TNT (Figure 1b) with MgO particles. We confirmed that these engineered materials absorb light with the energies considerably lower (and wavelengths considerably longer) than individual materials. We further showed that the presence of such distinct optical properties generated by interfaces is necessary but not sufficient for achieving optical initiation of the energetic materials. We will also discuss effects of stability of the ionized energetic molecules on the process of optical initiation and ways how the energy release from high energy density materials can be controlled for multiple novel applications.

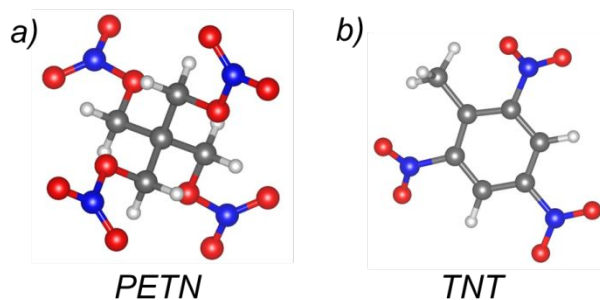


Figure 1. Schematics of the molecular structures of PETN and TNT. Carbon atoms are shown in gray, oxygen – in red, nitrogen – in blue, hydrogen – in white.

2 Methods

2.1 Details of calculations

Solid state periodic calculations were performed with density functional theory (DFT)^{40,41} using GGA PBE⁴² functional and projector augmented-wave (PAW) approximation⁴³, as implemented in the VASP code^{44,45,46}. In calculations of an ideal MgO bulk crystal (Figure S1 of Supplementary Information), the convergence criterion for total energy was set to 10^{-5} eV, and the maximum force acting on each atom in the periodic cell was set not to exceed 0.01 eV/Å. We used $3\times 3\times 3$ Monkhorst–Pack k -point mesh with the Gamma point in the center, and the kinetic energy cut-off was set to 520 eV. The calculated lattice constant of the cubic (rock salt) unit cell, $a=4.250$ Å, agrees with the experimental lattice vectors of $a=4.216$ Å⁴⁷ within 1%. To simulate a pristine MgO surface, we used a periodic slab model. A rectangular block of MgO four layers represented a supercell slab (Figure S2 of Supplementary Information) cut out from the bulk MgO structure to form the MgO surface with the (001) orientation, with the supercell lattice vectors of $a=b=17.0$ Å and $c=26.38$ Å. The vacuum layer of 20 Å placed on top of the (001) MgO surface was intended to minimize interactions between supercells in z direction and to ensure that electron density at translated slabs do not overlap. To correct the significantly underestimated band gap energies obtained from standard PBE, a self-consistent single point calculation was performed for each configuration by using hybrid PBE0 functional⁴⁸. Energies of PETN and TNT adsorption on MgO (001) surface were calculated using opt-PBE-vdW^{49,50,51,52,53} functional, which includes corrections for weak van der Waals interactions.

Embedded Cluster Method (ECM) calculations were performed using ORCA 4.0.1 program⁵⁴. In these calculations, MgO (001) surface was represented with a quantum cluster containing 50 atoms arranged in two atomic layers (Figure S2 of Supplementary Information). The quantum cluster (QC)

was cut out of the ideal relaxed MgO bulk crystal, and the atomic positions were kept fixed during calculations. A 65-atom layer was added to describe the quantum cluster boundary. Effective core potentials (ECP) and atomic charges (Mg (+2.0 e) and O (-2.0 e)) were assigned to each Mg and O atoms at the boundary layer to account for neglected repulsive terms at the border of the cluster⁵⁵. The quantum mechanical cluster surrounded by the boundary layer was then placed in the field of 1685 point charges (Mg (+2.0 e) and O (-2.0 e)). B3LYP^{56,57} density functional with 6-31G(d) basis set was used in the embedded cluster calculations. This way mimics rather well the *ab initio* model potential approach.

All *molecular calculations* in our study were carried out with the GAUSSIAN 09⁵⁸ program suite. Equilibrium ground state structures and energies of the highest occupied molecular orbital (HOMO) – lowest unoccupied molecular orbital (LUMO) gap were obtained using hybrid PBE0⁴⁸ functional with 6-31+G(d,p) basis set. Vertical excitation energies for the lowest singlet (S) and triplet (T) states were computed using time dependent TD PBE0 method^{59,60}.

2.2 Details of experiment

Diffuse reflectance spectra of MgO-PETN, MgO-TNT composites, and all pure components were measured by Shimadzu UV-3600 scanning spectrophotometer equipped with a UV-VIS-NIR integrating a sphere attachment ISR-3100. The magnesium oxide powder was mixed with one of the energetic materials (PETN or TNT) by grinding in an agate mortar. Concentrations of EMs in a mixture varied from 0.2 to several mass percent. The MgO-PETN and MgO-TNT mixtures were then heated in a drying cabinet above the melting point of each corresponding energetic material for 10 minutes to achieve a better coating of MgO particles by an energetic material. MgO-PETN samples were heated up to 143°C, and MgO-TNT samples were heated up to 87°C. The obtained diffuse reflection spectra were analyzed by using the Kubelka-Munk formula.

In the laser initiation experiments, PETN-MgO composite samples with PETN concentration of 1% wt. and TNT-MgO composite samples with TNT concentration of 1 and 5 % wt. were used. MgO-PETN and MgO-TNT samples were prepared by mixing MgO with PETN or TNT powders in hexane using an ultrasonic homogenizer. After hexane evaporation, MgO-PETN and MgO-TNT mixtures were pressed at a pressure of 0.4 GPa into the aperture of the holder. The holder had a shape of a disc and was made of stainless steel. Resulting samples were in the form of tablets of 3 mm in diameter and 1 mm in thickness. The mass of each tablet was 14 mg. Similar tablets were prepared for initiation of pure PETN and TNT samples. Densities of PETN and TNT samples were close to the density of single-crystal materials.

The holder with a sample was installed in the experimental setup as shown in Figure 2. The investigated samples were initiated by the first (1064 nm) and the second (532 nm) harmonic of laser radiation of a YAG: Nd laser LDLP10M (Laser Dream, China). LQ929 YAG:Nd laser (SOLAR Laser Systems, Belarus) was used for the third (355 nm) harmonic generation. The pulse duration of both lasers was 14 ns. The required energy density was achieved by a focusing lens and varying the applied voltage of the laser pumping lamps. The energy density was controlled by the pyroelectric energy meter PE50BF-DIF-C (Ophirspiricon, Israel). For precise determination of the energy density on the sample surface, a part of the beam passing through the empty holder aperture (without the sample) was measured. The empty holder without a base was fixed to the covering washer and placed in the same position as it was done in the initiation experiment.

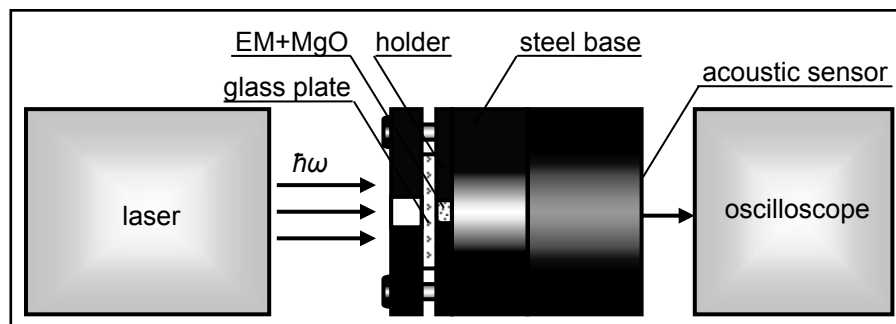


Figure 2. Experimental setup used for laser initiation of composite energetic materials

An advantage of the applied laser initiation technique is that it allows for safe and fast testing of a large number of samples under the same conditions. The limitation is that the configuration of the experimental setup does not provide an opportunity to study many different characteristics of the process. This fact motivated us to formulate a criterion of successful initiation that included an appearance of an intense acoustic signal and the explosion of the entire sample volume. The acoustic signal was registered by the piezo-sensor, and the completeness of the explosion reaction was evaluated visually by observing a fragmented (destroyed) sample in the holder of an explosive chamber.

Warning! Both energetic materials, PETN and TNT, are high explosives and have to be handled with caution. More details on handling these materials in experiments are provided in Supplementary Information.

The probability of a sample explosion as a function of the initiating energy density was measured based on tests of minimum of 10 samples for each energy density. The laser initiation threshold was determined as an energy density necessary for the successful initiation of at least 50% of samples.

3 Results

3.1 DFT modeling

3.1.1 *Electronic properties of individual materials and MgO-PETN and MgO-TNT interfaces*

The electronic structure of both bulk and surface magnesium oxide has been previously studied theoretically and experimentally^{61,62,63,64,65,66,67,68,69,70} in detail. The energy gap of the MgO bulk crystals is 7.78 eV⁴⁷. The electronic structure of MgO is characterized by a strong localization of valence electrons and a large band gap between occupied anion (O $2p$) and unoccupied cation (Mg $3s$) states³⁸. The band gap of the MgO is reduced from 7.78 eV in the bulk^{47,71} to 5.5 eV at the (001) surface plane⁷².

Optical properties of PETN and TNT were also thoroughly investigated individually and hence there is a great deal of data available for validation. In molecular calculations⁷³, the PETN HOMO is found to be a non-bonding orbital formed predominantly by p orbitals of oxygen atoms from nitro groups (Figure 3a). The quasi-degenerated HOMO-1, HOMO-2 and HOMO-3 are also non-bonding orbitals of a similar nature and lie only slightly below the HOMO. The LUMO is an anti-bonding π^* molecular orbital (Figure 3b) with a large contribution of p orbitals of nitrogen and oxygen atoms. The LUMO is followed by quasi-degenerated LUMO+1, LUMO+2 and LUMO+3 with the energy only slightly higher than the energy of the LUMO.

The absorption spectrum of PETN consists of three main bands at 193.5 nm (>6.41 eV), 260 nm (4.77 eV) and 290 nm (4.27 eV)^{73,74,75,76,77}. It is established that the excitation of gas-phase PETN molecules by a laser beam with energies of 5.0, 5.25, and 5.48 eV and pulse duration of 8 ns initiates decomposition releasing the nitric oxide as an initial product⁷⁵.

The HOMO of a TNT molecule (Figures 3c) is formed by the $2p_z$ states of C and O atoms. The LUMO state (Figure 3d) has a substantial contribution of the N $2p_z$ states in addition to $2p_z$ states of C and O atoms. Figures 5c and 5d show that the HOMO and LUMO states of TNT are smeared over an aromatic ring and nitro groups of the molecule. This property of the TNT LUMO has a strong effect on stability of the negatively charged molecule and plays a crucial role in the process of laser initiation, as it will be shown later.

The absorption spectrum of TNT has a low intensity peak at 326 nm (3.80 eV).⁷⁶ It corresponds to the lowest singlet-singlet transition. All other transitions occur at higher energies, as is shown by the broad absorption band between 4.5 and 6 eV.⁷⁶

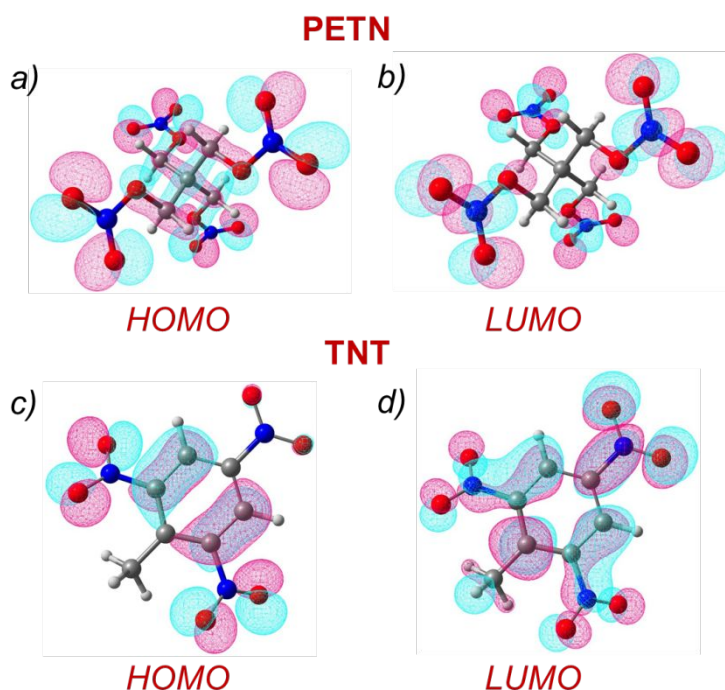


Figure 3. Molecular orbitals of PETN and TNT. Carbon atoms are shown in gray, oxygen – in red, nitrogen – in blue, hydrogen – in white. Positive part of a molecular orbital is shown in magenta, negative – in and cyan.

In modeling PETN adsorption on the MgO surface, three most plausible configurations (Figures 4 a-c) were probed. In these configurations, a PETN molecule interacts with an oxide

surface via one, two, or three $-O-NO_2$ tails, respectively. The lowest adsorption energy (-12.8 kcal/mol) was obtained for *Configuration I* with the PETN molecule adsorbed via one $-O-NO_2$ tail. In *Configuration II*, the PETN molecule adsorbs slightly stronger (by 8.6 kcal/mol) via its two $-O-NO_2$ tails. Consistently, *Configuration III* in which PETN interacts with the oxide surface via three $-O-NO_2$ tails has the highest adsorption energy (-26.3 kcal/mol).

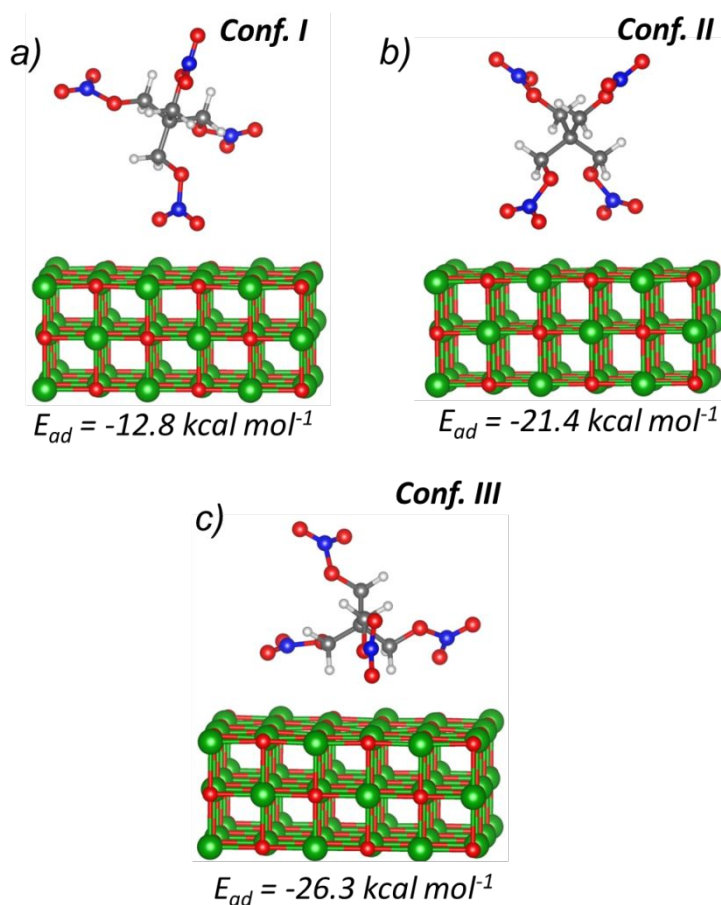


Figure 4. Schematics of the adsorption of PETN molecule on MgO (001) surface. Carbon atoms are shown in gray, oxygen – in red, nitrogen – in blue, hydrogen – in white, magnesium – in green.

When PETN is adsorbed on the MgO (001) surface, new electronic states appear in the MgO band gap (Figure 5a) that lie 3.5 - 3.7 eV above the MgO valence band maximum. These new states are localized on $-O-NO_2$ tails of PETN (Figure 5b) and formed by $2p$ functions of oxygen and

nitrogen atoms. The top of the valence band of PETN-MgO interfaces is localized on oxygen atoms of MgO (Figure 5c). Imaginary parts of the frequency dependent dielectric matrix (Figures 5 d-f), calculated and plotted for the three adsorption configurations of PETN on MgO (shown in Figures 4 a-c), exhibit little difference between the probed configurations, which is consistent with the closely positioned electronic states in the band gap (Fig. 7a, 3.34 – 3.69 eV). These plots have distinct low intensity shoulders with the energies of 3-4 eV. Because neither PETN nor MgO can absorb light with such low energies, these weak transitions appear only at interfaces between energetic material and metal oxide.

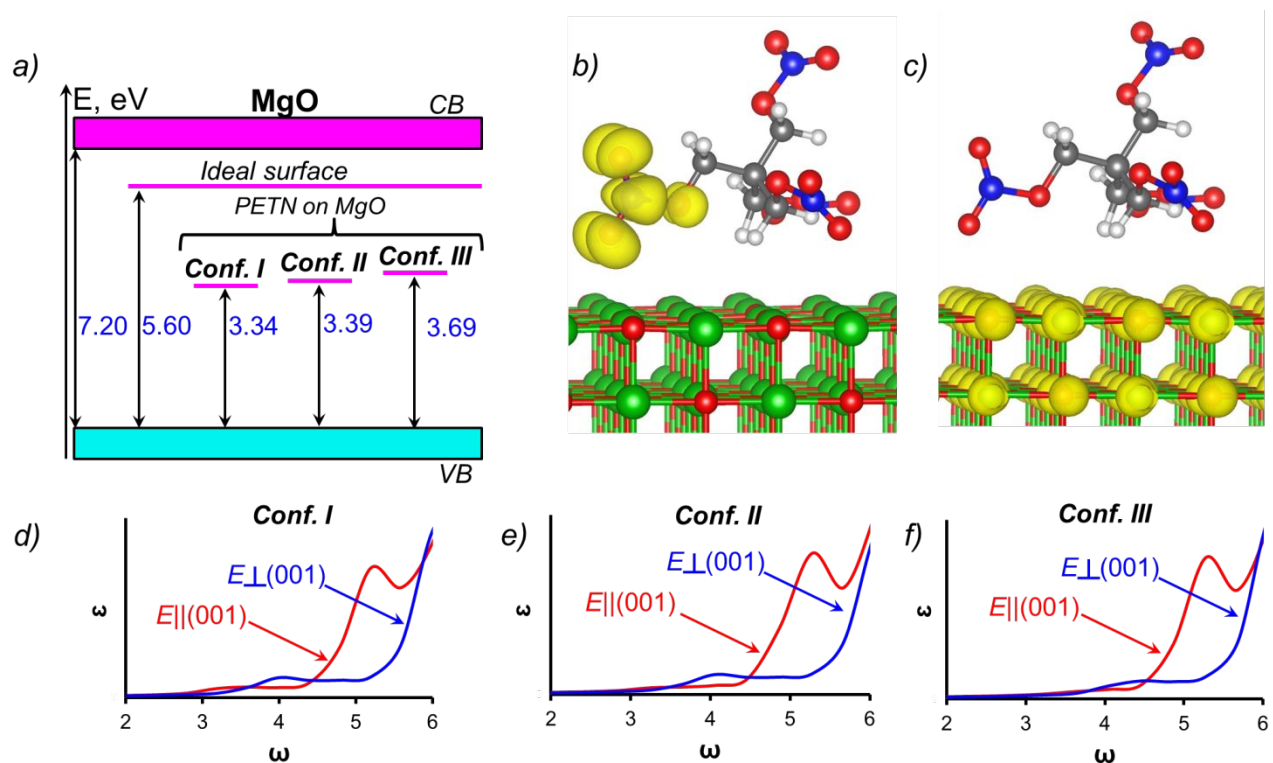


Figure 5. a) Energy diagram shows relative positions of vacant electronic levels of PETN in the energy gap of MgO, b) Charge density of the lowest unoccupied state of MgO-PETN interfaces c) Charge density of the top of the valence band of MgO-PETN interface, d-f) An imaginary part of the dielectric constant calculated for three different adsorption configurations of PETN on MgO. Some explanations for b) and c) are needed. Carbon atoms are shown in gray, oxygen – in red, nitrogen – in blue, hydrogen – in white, magnesium – in green.

In modeling TNT adsorption on MgO surface, we took in consideration four plausible configurations shown in Figure 6 a-d. In *Configuration I* (Figure 8a), the TNT molecule is adsorbed horizontally to the surface. This configuration corresponds to the highest adsorption energy (32.7 kcal/mol). In the three remaining configurations (Figures 6 b-d), the TNT molecule is adsorbed vertically and interacts with the surface via one or two nitro groups. These are less favorable configurations with the adsorption energies (15-18 kcal/mol) considerably (~2 times) lower than in *Configuration I*.

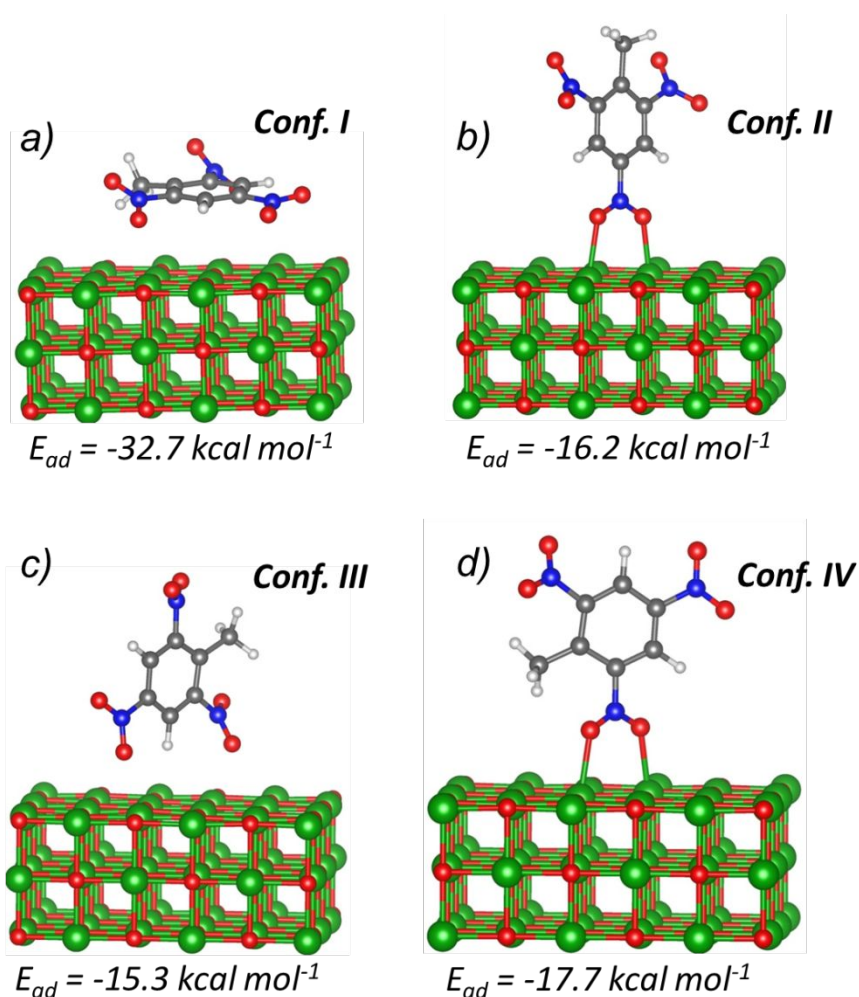


Figure 6. Adsorption of TNT on MgO surface. Carbon atoms are shown in gray, oxygen – in red, nitrogen – in blue, hydrogen – in white, magnesium – in green.

Similarly, to the PETN-MgO interface, new electronic states in the MgO energy gap appear upon adsorption of TNT on the MgO (001) surface (Figure 7a). These new states lie 2-2.6 eV above the MgO valence band maximum and are localized on the TNT molecule (Figure 7b). The valence band maximum of the TNT-MgO interface is localized on oxygen atoms of MgO. The imaginary parts of the frequency dependent dielectric matrix plotted for different adsorption configurations of TNT on MgO (Figure 7 d-g) shows that TNT-MgO interfaces can absorb light in the energy range of 2-3 eV, which is significantly lower than onset of absorption of the pristine individual materials.

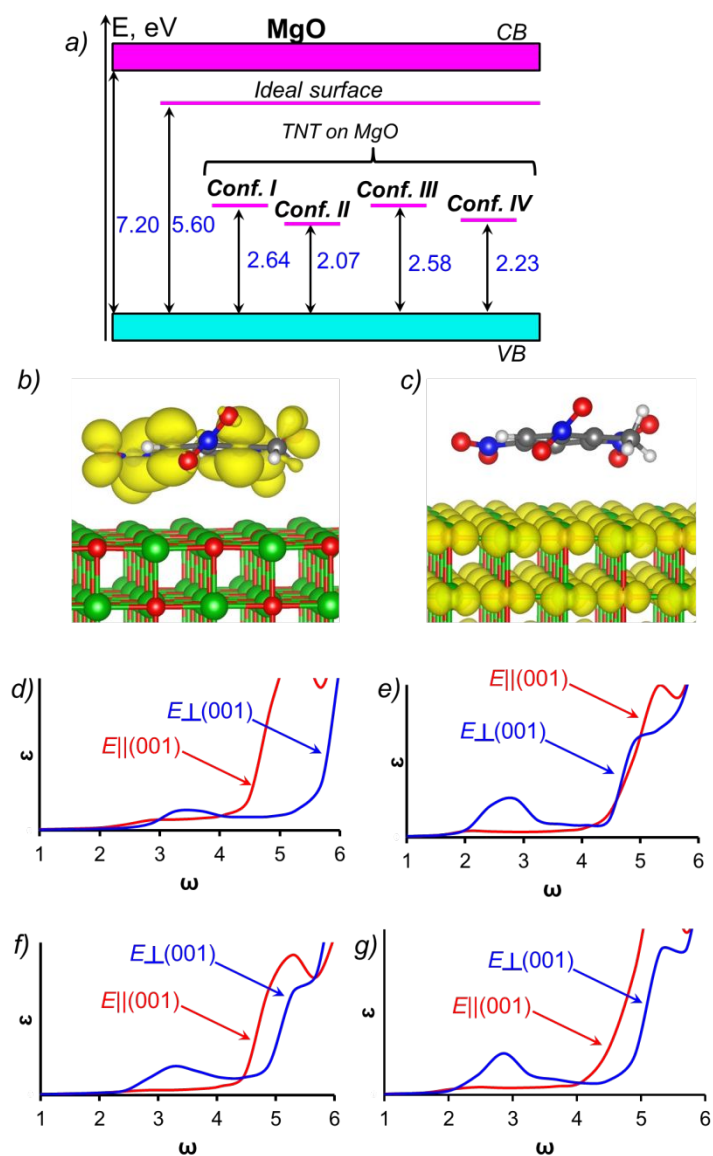


Figure 7 a) Energy diagram showing positions of vacant electronic levels of TNT in the energy gap of MgO, b) charge density of the lowest unoccupied state of the MgO-TNT interface, c) charge density of the top of the valence band of the MgO-TNT interface, d-g) an imaginary part of the dielectric constant calculated for adsorption of three different adsorption configuration of PETN on MgO. Add explanations for (b) and (c). Carbon atoms are shown in gray, oxygen – in red, nitrogen – in blue, hydrogen – in white, magnesium – in green.

Our calculations revealed strong adsorption of PETN and TNT molecules on MgO, which means that mixing these molecular materials with MgO will result in forming many interfaces in the engineered samples. PETN-MgO and TNT-MgO interfaces demonstrate distinct optical properties that are, indeed, promising for triggering chemical reactions through optical excitation. However, this finding requires a careful validation and further analysis. Hence, we will use the embedded cluster approach to validate our conclusions and analyze the nature of optical transitions.

3.1.2 Validation using an embedded cluster approach

An embedded cluster methodology allows one to include a single defect (in our case, an excited state, or explicitly a single electronic transition) in the quantum cluster. This approach is different from the periodic model in which electronic density of defects located in the neighboring periodic supercells may overlap, which could generate some artificial features. Hence, we hypothesize that results obtained in the previous section are reasonable if the envisioned embedded cluster model calculations produce the same conclusions for defect related optical absorption bands at the interfaces.

Prior to modeling of the adsorption of energetic molecules and calculating energies of electronic transitions, we conducted a series of test calculations to check how well our cluster model can reproduce the basic electronic properties of the MgO surface (See Table S1 of Supplementary Information for more detail). The HOMO-LUMO gap of the MgO cluster (5.65 eV), obtained from

the embedded cluster approach and B3LYP functional, is in good agreement with the experimentally measured energy gap of the MgO (001) surface of 5.5 eV⁷².

The energy of the lowest S_0 - S_1 transition, calculated using TD B3LYP, is 5.0 eV, which agrees with the early TD DFT estimation of 5.3 eV⁶⁴ and is slightly lower than experimental estimates⁷². According to earlier work by Sushko⁶⁴, TD DFT tends to systematically underestimate energies of the vertical electron transitions in MgO. Finally, the B3LYP-calculated ionization potential of the MgO surface (6.46 eV) was found in agreement with the earlier DFT calculations (6.7 eV)⁶³ and experimental measurements (\sim 6.2 eV)⁷². Overall, these comparisons confirm that the employed embedded cluster method reproduces electronic features of MgO reasonably well. The observed small difference with earlier calculations^{63,64} is due to differences in details of the implemented ECM methods (e.g., a size of the quantum cluster, a number of point charges describing the Madelung field, embedding potentials, etc.).

In calculations of adsorption of nitro molecules on the MgO (001) surface by the ECM approach, we replaced PETN and TNT molecules with their simulant compounds: ethyl nitrate (EN, Figure 8a) and o-nitro toluene (NT, Figure 8b), respectively. Our previous study⁷³ showed that the simulant compounds can be effectively used to explore optical properties of the real energetic molecules because optical and electronic properties are fully determined by the type of the functional groups (e.g. -ONO₂ and -NO₂) but not by their number.

Adsorption configurations of EN and NT on MgO cluster are shown in Figures 8 c and 10 d. Electronic properties of the MgO (001) surface and MgO interfaces with nitro compounds calculated by the embedded cluster model and periodic method are compared in Table 1. The HOMO-LUMO gap of the MgO cluster calculated with B3LYP functional (5.65 eV) is in excellent agreement with the energy gap obtained from periodic calculations with PBE0 method (5.60 eV). Once the EN

molecule is adsorbed on the MgO surface, EN-generated vacant electronic states appear in the MgO energy gap. The HOMO-LUMO gap (obtained from B3LYP) of this system is 3.61 eV. This agrees well with the position of the vacant electronic PETN states in the energy gap above the top of the MgO valence band (3.34-3.69 eV Figure 5a, Table 1, obtained with PBE0). The energy of the lowest S_0 - S_1 excitation in MgO-EN system obtained TD B3LYP is 2.91 eV. This excitation is associated with the transition of an electron from the top of the MgO valence band to the lowest unoccupied state of EN. Note, this transition has non-zero oscillator strength and, therefore, should be detected in experiments on optical absorption.

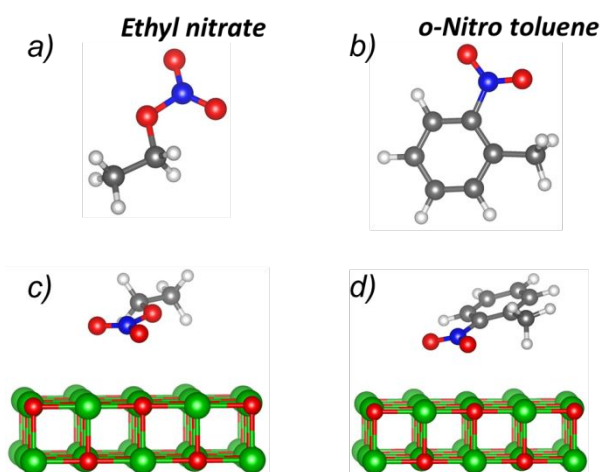


Figure 10 The molecular structures of a) ethyl nitrate and b) o-Nitro toluene; adsorption of c) ethyl nitrate and d) o-Nitro toluene on the MgO quantum cluster. Carbon atoms are shown in gray, oxygen – in red, nitrogen – in blue, hydrogen – in white, magnesium – in green.

Similar to EN adsorbed on MgO, vacant electronic states of an NT molecule appear in the energy gap of the MgO (001) surface. The NT LUMO is located 2.79 eV (B3LYP) above the HOMO of the MgO cluster. This is consistent with the position of the TNT states above the top of the MgO valence band (2.07-2.64 eV, Figure 7a, Table 1) obtained from solid state periodic calculations with

PBE0 functional. The lowest S_0 - S_1 excitation (calculated with TD B3LYP) has the energy of 2.13 eV and is associated with the electronic transition from the MgO cluster's HOMO to the LUMO of NT.

Table 1. Electronic properties of the MgO (001) surface and MgO interfaced with nitro molecules obtained from the embedded cluster model and periodic calculations.

Embedded cluster model calculations (B3LYP)			Periodic calculations (PBE0)		
System	Feature	Energy (eV)	System	Feature	Energy (eV)
MgO (001) surface	HOMO-LUMO	5.65	MgO (001) surface	Band gap	5.60
	S_0 - S_1 ^a	5.0			
MgO-EN	HOMO-LUMO	3.61	MgO-PETN	HOMO-LUMO	3.34-3.69 ^b
	S_0 - S_1	2.91			
MgO-NT	HOMO-LUMO	2.79	MgO-TNT	HOMO-LUMO	2.07-2.64 ^c
	S_0 - S_1	2.13			

^a Energies of vertical electronic S_0 - S_1 transitions were obtained using TD B3LYP method, ^b for three probed configurations shown in Fig. 4; ^c for four probed configurations shown in Fig. 6.

Our modeling, performed by both periodic supercell calculations and embedded cluster method calculations, shows that the vacant electronic states of the nitro molecules fall in the energy gap of the EM-MgO (001) interface. This results in the new optical transitions associated with the electronic excitation from the top of the MgO valence band to the lowest unoccupied states of the molecules. A comparison between two methods vividly demonstrate that both the nature and the energies of the obtained electronic transitions are in remarkable agreement. Hence, they represent a real physical situation and are not a deficiency of the chosen methodology or a computational scheme. We further develop a feasible mechanism of the photo-stimulated decomposition of the nitro molecules on a MgO surface.

3.1.3 Photo-stimulated decomposition mechanism

We propose the following mechanism of photo-initiated chemical decomposition of the EM-MgO samples. We emphasize here that the decomposition we aim to achieve with a low energy optical excitation occurs only at the engineered EM-MgO interfaces and does not happen in the isolated EM molecules or pristine EM solids. The first step in the EM decomposition process (Figure 9) is an electronic excitation from the MgO valence band maximum to the lowest unoccupied state of the PETN or TNT molecule. Such an electronic excitation is triggered by a direct low energy optical absorption of the interface. This is accompanied by the charge transfer from the MgO surface to the energetic molecule and results in the formation of the anion radicals of PETN or TNT. Nitro-compounds have high electronic affinity and readily trap an electron if it appears in the vicinity. The second step is the actual decomposition of the PETN and TNT anion radicals. Our previous study discovered that the decomposition of the PETN anion radical via the O-NO₂ bond cleavage requires only 18 kcal/mol³⁸, which is twice lower than the energy required for the decomposition of a neutral ground state PETN molecule, ~35 kcal/mol^{78,79}. We found it interesting that unlike PETN, the decomposition of both the ground state TNT molecule and TNT anion radical ion requires close energies of ~50 kcal/mol^{80,81}. Hence, the photo-stimulated decomposition of PETN on MgO is favored over an ordinary thermal decomposition of pristine PETN while there is no significant difference in ways triggering decomposition of TNT.

The relative stability of the TNT anion radical versus instability of the PETN anion radical can be explained by the significantly different nature of valent orbitals of the PETN and TNT molecules and different distribution of charges on the ion radicals. As it has been mentioned before, the LUMO of PETN is anti-bonding π^* orbital localized on the O-NO₂ groups (Figure 3b). In the PETN anion radical, an extra electron is localized on one -O-NO₂ tale (Figure 10a). As a result, the

O-NO₂ bond breaking in the PETN anion radical requires a significantly lower energy than in the neutral ground state molecule. Unlike PETN, an extra electron in TNT anion radical is uniformly delocalized over its aromatic ring and nitro groups (Figure 10b). Such a delocalization of the extra electron has a strong stabilizing effect on the TNT molecule, precluding its decomposition.

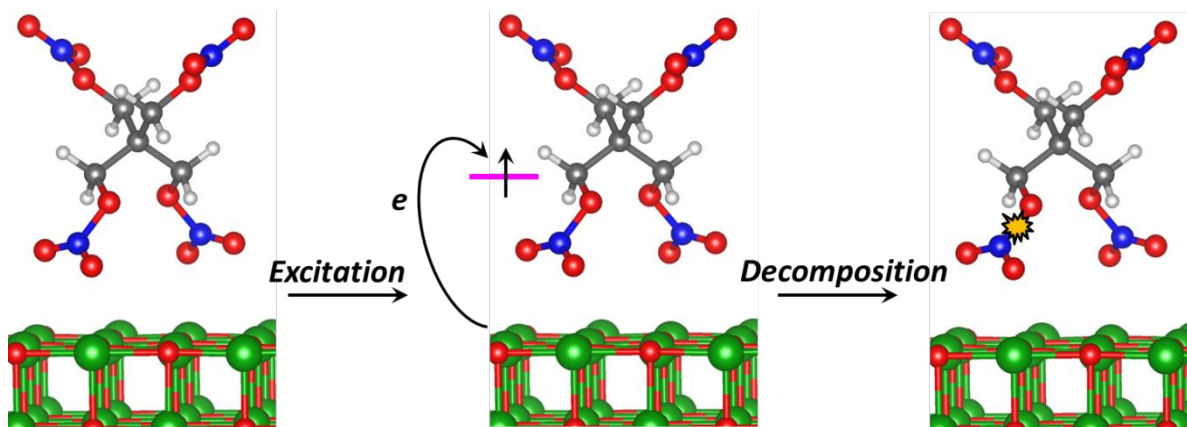


Figure 9. Mechanism of the photo-initiated chemical decomposition of PETN-MgO samples. Carbon atoms are shown in gray, oxygen – in red, nitrogen – in blue, hydrogen – in white, magnesium – in green.

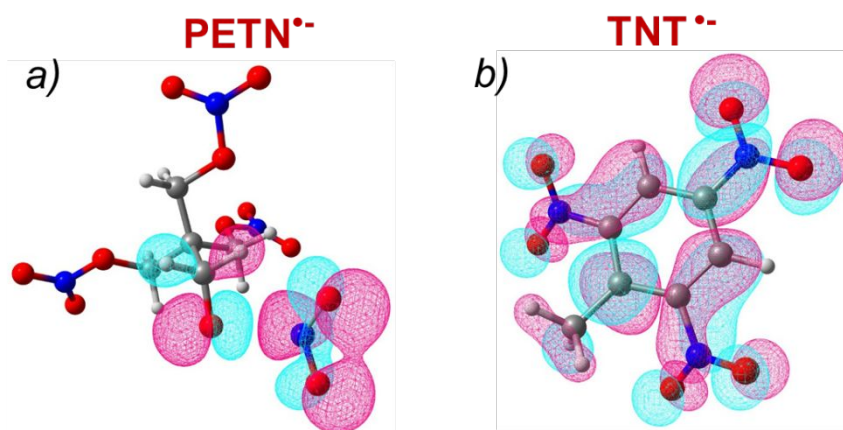


Figure 10. Electron component in a) PETN and b) TNT anion radicals. Carbon atoms are shown in gray, oxygen – in red, nitrogen – in blue, hydrogen – in white. Positive part of a molecular orbital is shown in magenta, negative – in and cyan.

Summing up, our calculations show that PETN and TNT molecules are strongly adsorbed on the MgO (001) surface, forming engineered interfaces with visibly different electronic, optical, and chemical properties than the separated individual material components. For example, both MgO and all energetic materials are wide band gap dielectrics with a bandgap of 6-7 eV or higher. In the meantime, EM-MgO compounds absorb energies of ~ 2.5 - 3.5 eV. This is because the energetic molecules adsorbed on the MgO surface generate vacant electronic states in the energy gap of the EM-MgO system. This results in a series of the distinct optical transitions corresponding to electron excitations from the MgO valence band to the lowest unoccupied states of the molecules. These transitions have energies noticeably lower than adsorption edge of the individual materials. The electronic transitions cause the charge transfer from the metal oxide to the molecule leading to the formation of the PETN and TNT anion radicals with different thermal stability. Our analysis leads us to predict that the PETN-MgO and TNT-MgO interfaces will absorb light with the energies of ~ 3.5 and ~ 2.5 eV, respectively. Such a low energy stimulated excitations will trigger explosive decomposition of these composites, which opens completely new opportunities in controllable release of energy that is stored in EM in large quantities. At the same time, we found that the PETN-MgO interfaces demonstrate much higher sensitivity to optical initiation than the TNT-MgO samples. The discussion above has a qualitative character. While we argue that the suggested mechanism of excitation triggered decompositions is logical and feasible, studies on the dynamics evolution of the system in the excited state with an explicit modeling of chemical reactions are required to prove and further validate the possibility of such a decomposition scenario.

3.2 Experiment

3.2.1 Light absorption of the PETN-MgO and TNT-MgO interfaces

The goal of our measurements is to register optical absorption of EM-MgO interfaces to confirm our theoretical findings and compare the measured energies with our DFT calculations that found low subband energy electronic excitations realized at interfaces.

The measured reflection spectra of the pure MgO and PETN powders are shown in Figure 11a. Pure PETN doesn't absorb light with the energy lower than 4 eV, which is in good agreement with earlier experiments^{39,74} and our calculations (see Table 1). MgO begins absorbing light with energies higher than 5 eV, also consistent with the calculations (Table 1). The reflection spectrum of TNT (Figure 11b) has a low intensity shoulder at energies between 2 and 3 eV and two distinct maxima of higher intensity at 3.5 and 6.2 eV.

The reflection spectrum of the PETN-MgO interface (Figure 11c) has distinct absorption in the energy range of 2-4 eV that are not observed in the spectra of individual materials (Figure 11a). Two new absorption bands with maxima of 3.1 and 4.2 eV are clearly distinguished. The 3.1 eV maximum is consistent with the calculated absorption energies (3.34 – 3.69 eV, Figure 5a) of various configurations of PETN molecules adsorbed on MgO surfaces and the energy of singlet-singlet transition (2.91 eV, Table 1). The curve shape of the MgO-PETN spectrum correlates well with the graphs of the calculated imaginary part of the dielectric constant represented in Figures 5 d-f.

The reflection spectra obtained for TNT-MgO composite samples (Figure 11d) have distinct maxima at ~1.7 and 2.5 eV. These bands also can not be explained by the absorption of the individual components, pure TNT or MgO. However, they are consistent with the calculated absorption energies (2.07-2.64 eV) of TNT molecules in various configurations adsorbed on the MgO surface (Figure 7b) and the energy of singlet-singlet transition (2.13 eV, Table 1).

Thus, our experiments on optical absorption of MgO-PETN and MgO-TNT composite samples revealed new distinct absorption bands, which were not observed in the reflection spectra of the individual materials. Accordingly, MgO-PETN samples absorb light with the energy as low as 3.1 eV, whereas the reflection spectrum of MgO-TNT samples has two new distinct bands at 1.7 and 2.5 eV. These findings are in good agreement with the results of our DFT modeling and lend an additional support to the conclusions obtained from our computational modeling.

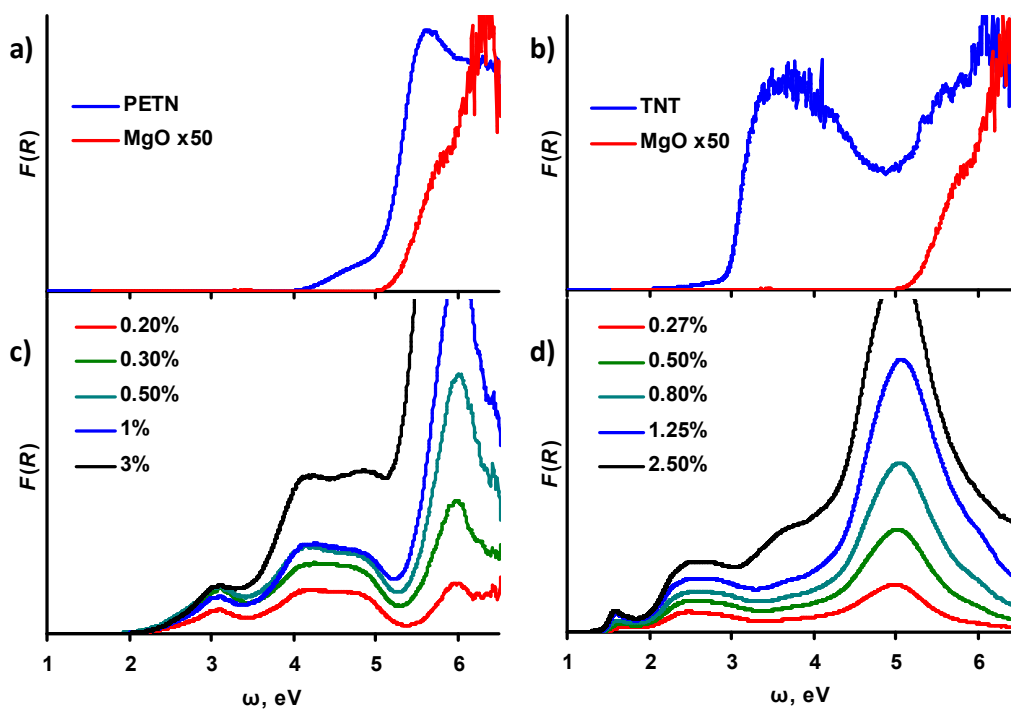


Figure 11. The diffuse reflectance spectra Kubelka-Munk function of: a) individual PETN and MgO components, b) individual TNT and MgO, c) PETN – MgO composite for various PETN concentrations, and d) TNT–MgO composites for various TNT concentrations.

3.2.2 Laser photo initiation of the PETN-MgO and TNT-MgO composites

The measurements of photo initiated explosive chemical decomposition reactions aimed at identifying the energy density thresholds for each laser irradiation harmonic and at looking for any differences in initiation of TNT-MgO vs PETN-MgO. Based on our computational modeling, we hypothesize that the chemical reaction in TNT-MgO would be more difficult to initiate than in

PETN-MgO. In addition, we expect that there should be a pronounced difference in initiating pure PETN vs PETN-MgO, while there should be barely any difference in initiating pure TNT vs TNT-MgO.

The energy density threshold of the initiation of the pristine PETN samples by 1064 nm (1.17 eV, first harmonic) and 532 nm (2.33 eV, second harmonic) wavelengths is 3.1 J/cm² (Figure 12). We were not able to achieve the laser initiation threshold by a third harmonic with the wavelength of 355 nm (3.49 eV) under applied experimental conditions. Figure 12 shows that the probability of initiation is only 10% at the maximum possible energy density of 2.1 J/cm². All three harmonics probed, including the third harmonic of YAG:Nd laser (355 nm), are within the transparency region of PETN. It was shown that the laser initiation thresholds of PETN are rather close for all three long-wavelength harmonics. The required energy density flow dramatically decreases only with the use of Xe-Cl excimer laser (308 nm, 4.03 eV)⁸² and YAG:Nd fourth harmonic (266 nm, 4.66 eV)⁸³, which nearly coincides with PETN absorption at 4.77 eV and is consistent with our DFT calculations. Therefore, it is reasonable to assume (for simplicity) that the threshold for 355 nm wavelength, under our experimental conditions, also is not much different from thresholds for other harmonics and it is about 3 J/cm².

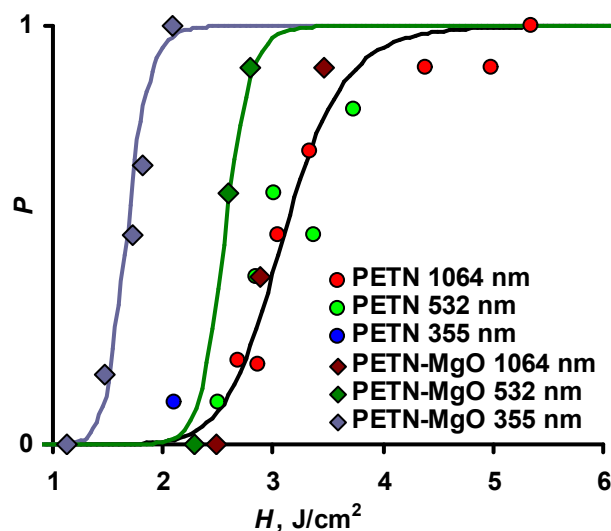


Figure 12. The explosion initiation probability of PETN and PETN-MgO composite as a function of the energy density.

In exploring PETN-MgO composites, we found that an addition of 1% wt. MgO only slightly affects the energy density threshold of laser initiation by 1064 nm wavelength. The threshold of initiation by 532 nm is decreased (more than for the first harmonic) to the value of 2.6 J/cm², and the threshold by 355 nm is significantly decreased to 1.7 J/cm². We reiterate here that a maximum decrease in the threshold of the laser initiation is achieved for the irradiation wavelength, which falls into the transparency region of both the pure energetic material and the additive. This observation is consistent with the PETN-MgO interface absorption band, predicted in DFT calculations.

We suggest the following interpretation of these observations. We will start with the third harmonic as it offers the most vivid illustration. While the laser initiation threshold by the third harmonic (355 nm, 3.49 eV) was not even achievable in our experiments with pristine PETN, PETN-MgO samples were initiated with much lower required energy exposure (1.7 J/cm²) than other harmonics. The excitation energy of this harmonic (3.49 eV) corresponds to the optical absorption

energy of PETN-MgO of 3.34 – 3.69 eV (see Table 1 and Fig. 5a) and indicates that this optical excitation effectively perturbs and dissociates the O-NO₂ bonds in PETN at the interface. This serves as a precise tool to trigger the energy release from PETN in a targeted and highly controllable way.

A barely noticeable decrease in the registered energy threshold by the first harmonic (1064 nm, 1.17 eV) initiation is also logical and rather expected if we recall that the low energy absorption is associated with an electronic excitation of F-centers on MgO³⁸. Earlier, we proposed that the optical transition (accompanied with a charge transfer) from a MgO F-center to PETN, which prompts decomposition of PETN, requires only 1.3 eV, very close to 1.17 eV³⁸. Apparently, this process occurs only at the interface and is characterized by a low probability that strongly depends on the concentration of oxygen vacancies in the sample. In our current absorption measurements (Figure 11), the PETN-MgO samples start absorbing energy higher than 2 eV. We suggest however that this does not contradict our earlier conclusions^{30,31,38} and is related to differences in sample preparation methods used. Our current samples had much lower concentration of oxygen vacancies and therefore the low energy absorption (1.17 eV) can not be effective here. This explains that the decrease of the energy threshold is barely noticeable for the first laser harmonic.

Interpolating this analysis to the second harmonic (532 nm, 2.33 eV) threshold decrease, one should expect that the absorption and the consequent bond dissociation is also activated by structural and/or electronic MgO surface defects and their interactions with PETN. There are numerous arguments to provide evidence^{36,37,84} that supports this notion.

An increase of a slope of the probability curve also serves as a good indication of a change of the initiation mechanism. Earlier, we proposed a fluctuation model of the EM laser initiation⁸⁵, which connects a slope of the linear part of the probability curve with the hot-spot (explosion reaction origination sites) formation effectiveness. Assuming a stochastic nature of the hot-spot formation in

pure PETN, one should conclude that it is not effective (that is there are only a few random sites at which reaction is initiated) as reflected in a small slope of the curve, illustrating a low probability of the explosion in the pristine material. The addition of 1% MgO causes a steep increase of the linear part of the probability curve, which becomes practically vertical for the initiation by the second and third harmonics. In terms of hot-spot (i.e., reaction origin) formation, this behavior clearly points to a switch of mechanisms when a much more effective way of reaction initiation becomes dominating. For example, at low energy (first harmonic), only sites involving oxygen vacancies at MgO-PETN are playing a role in initiation, and the probability of the explosion, while higher than at pristine PETN, is still rather low. With the second harmonic, other surface defects at MgO-PETN are additionally turning on, showing a significant increase in probability. With the third harmonic, the irradiation energy is sufficient to excite any PETN molecule at the interface and, therefore, initiation at all PETN-MgO reactive sites contributes to the overall PETN decomposition, showing 100% probability of explosion.

All our attempts to initiate pure TNT samples as well as the TNT composites with 1% MgO by 1064 and 532 nm laser radiation with the energy density as high as 5 J/cm² failed. An acoustic signal indicated that the laser pulse with the energy close to 5 J/cm² is capable of igniting the surface layer only. Unfortunately, the exposed energy is not sufficiently high to initiate the reaction in the whole sample volume; but it damages the cover glass plate. These observations agree well with the stability modeling of TNT anion radical. As a possible additional reason for the unsuccessful initiation, we explored whether it can be due to an extremely high extinction coefficient of the TNT samples to a large extent caused by the scattering. We tried to estimate the role of MgO in the laser ignition reaction by analyzing the acoustic signal using the composite containing 5% MgO. The threshold energy density and intensity of an acoustic signal coming from 5% MgO-TNT composite

turned out to be identical to results for pure TNT samples (Figure 13). Apparently, MgO additives hardly affect the TNT laser ignition, and the registered acoustic signal is a result of the ignition of a surface layer caused by the optical breakdown.

We conclude that despite an intensive absorption of MgO-TNT at the 532 nm wavelength, the laser excitation does not initiate decomposition of the composite. Therefore, optical initiation of MgO-TNT is not effectively applicable to control the energy release from TNT due to its remarkable stability. TNT anion radicals formed at the MgO-TNT interface exhibit similar high stability as pure TNT crystals and neutral ground state TNT molecules.

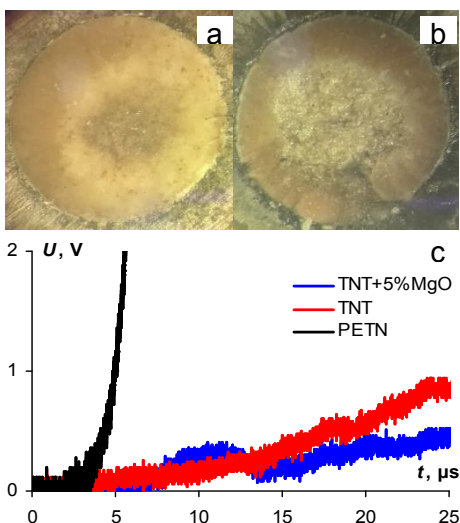


Figure 13. Photographs of the effects of irradiation of a sample of pure TNT (a), a sample of TNT with 5% MgO (b), and the corresponding acoustic response waveforms (c), a waveform of PETN initiation is given for comparison.

4 Discussion

We have conducted a joint experimental and theoretical study aimed at revealing mechanisms of photo initiation of composite high energy density materials that were prepared by mixing PETN or TNT explosives with crystalline MgO. Our ultimate goal is to understand whether the controllable energy release from high energy density materials can be achieved, for example, by engineering

materials interfaces or designing materials composites with tailored properties and functionalities. We argue that interfacing metal oxides with energetic materials is the most promising direction in such research.

Using a combination of DFT periodic calculations, embedded cluster method modeling, and optical absorption spectra measurements we discovered that both PETN-MgO and TNT-MgO composite interfaces absorb light with the energies much lower than the fundamental band gap of either the energetic materials or MgO. According to our calculations, absorption of low energy photons by the PETN-MgO and TNT-MgO engineered interfaces becomes possible due to distinct electronic states localized on PETN and TNT molecules and situated 3-3.7 eV (for PETN-MgO) and 2-2.6 eV (for TNT-MgO), respectively, above the valence band maximum. The corresponding calculated energies of optical transitions agree well with the absorption spectra energies observed in our experiments.

We further found that the laser excitation serves to initiate the explosive decomposition reaction of PETN-MgO and we proposed a logical mechanism of such initiation. Our laser initiation experiments combined with DFT modeling established that the most efficient initiation is triggered by the third harmonic (355 nm, 3.49 eV), which turned out to be consistent with the interface induced electronic transitions in PETN-MgO. On the other hand, initiation by the second (532 nm, 2.33 eV) and first (1064 nm, 1.17 eV) harmonics are largely associated with chemistry triggered on structural or electronic oxide surface defects. While they also contribute to initiation of chemistry at PETN-MgO interfaces leading to bond dissociation, the probability of the reaction is lower and strongly depends on the concentration of defects. At the same time, the morphology of the oxide surface can be deliberately manipulated by materials design and synthesis techniques to prepare a desired

interface with tailored chemical composition and defect content. Thus, laser initiation provides an efficient and reliable tool to extract energy from PETN in a highly controllable manner.

Interestingly, our calculations suggested that TNT-MgO interfaces will also absorb sub band photons, but this excitation will not lead to the explosive chemical reaction because the laser irradiation energy is not high enough. This conclusion was confirmed and validated by the optical absorption spectra measurements and laser initiation experiments in which it was possible to trigger only a surface dissociation reaction, but not decomposition in the entire TNT-MgO sample. We were also able to propose a consistent explanation of differences in dissociation of PETN⁻ and TNT⁻ ion radicals that is reflected in the measurements. Thus, we suggest that the low energy laser initiation of TNT-MgO interfaces is not efficient to release energy from TNT. Because of remarkable stability of TNT molecules, crystals, and TNT⁻ anion radicals, interfaces with MgO have little effect on reducing the threshold of initiation for TNT as much higher energies are required.

We note here that our calculations are based on rather simplified ideal surface/interface models that neglect any influence of structural defects and real surface morphology. We deliberately limited our study because the most efficient laser initiation of chemistry in the PETN-MgO samples was achieved with the third harmonic generation, which does not require defects. However, we argue that reactions photo-stimulated by the first and second harmonics are triggered on defects. It is well-known that structural defects (e.g., oxygen vacancies) at the MgO surface produce a wealth of distinct electronic levels in the fundamental band gap⁶⁴. Certainly, it would be interesting to study in more detail an effect of various structural defects (and particularly, oxygen vacancies and F-type centers) on the electronic properties of PETN-MgO and TNT-MgO interfaces as they likely to provide additional opportunities to control chemistry at even lower optical excitation energies as was clearly demonstrated in our earlier papers^{38,39}.

Results of this work lead us to formulate important criteria for making composite materials with tunable optical sensitivity. First, composite materials should have distinct optical properties, which would allow for an electronic excitation from the metal oxide valence band to an unoccupied state of explosive molecules. This optical transition would be stimulated by sub band laser irradiation, characterized by rather low energy. Second, such an excitation will drive the EM-oxide interface to the dissociation term through excited or charged state. However, we also established that achieving the desired optical and electronic properties in composite materials is not sufficient for successful initiation of decomposition reactions. Third, overall success depends also on electronic properties of the energetic molecule as well as on stability of its anion radical (at least for nitro-compounds that are usually electron deficient). According to our results, LUMO state of the energetic molecule needs to be localized on a particular functional group, X-NO₂ for nitro compounds and should demonstrate anti-bonding properties.

Conversely, energetic materials with tunable optical sensitivity can be prepared by adding a small portion of targeted metal oxides that add a desirable functionality to obtained interfaces. These results are essential for improving and miniaturizing optical detonators and enabling novel technologies that use lasers for initiation of energetic materials. Distinct optical properties observed on interfaces of metal oxides and energetic materials can be also used for sensing and detecting high explosives, for safe inexpensive cleaning of land and water that were exposed to toxicity of explosives, for safe mining and other purposes. Perhaps, most importantly, the obtained conclusions, indeed, offer new perspectives in using high energy density materials for a much broader range of common energy applications than it is usually envisioned and realized.

5 Conclusions

Our density functional theory and embedded cluster method calculations were combined with measurements of the optical absorption spectra and laser initiation experiments to explore how a controllable energy release from high energy density materials can be stimulated. We found that first (1064 nm, 1.17 eV), second (532, 2.33 eV), and third (355 nm, 3.49 eV) laser harmonics, to all of which pure energetic materials are transparent, can be effectively used to trigger explosive decomposition reactions in the PETN-MgO samples. The unusually low excitation energy that is able of initiating the reaction is achieved due to design of interfaces and suggests that the deliberately prepared surfaces and interfaces offer ways to safely extract chemical energy from high energy density materials. At the same time, TNT-MgO samples behave very differently. Similar to PETN-MgO samples, TNT-MgO were discovered to effectively adsorb sub band optical energy. Unlike PETN-MgO, TNT-MgO are highly resistant to initiate explosions due to high stability of TNT. We argue that this work opens fundamentally new perspectives on the use of high energy density materials for both basic and applied research.

Acknowledgements

This research is supported in part by National Science Foundation (NSF), Department of Energy (DOE), University of Maryland, and Russian Foundation for Basic Research (RFBR). RT and MMK acknowledge support of computational resources from NSF XSEDE (Grant DMR-130077), DOE NERSC (Contract DE-AC02-05CH11231), the Maryland Advanced Research Computing Center (MARCC), and University of Maryland (<http://hpcc.umd.edu>). ASZ was supported by RFBR (project #19-33-60013). MMK is grateful to the Office of the Director of National Science Foundation for support under the Independent Research and Development program. Any appearance of findings,

conclusions, or recommendations expressed in this material are those of the authors and do not necessarily reflect the views of NSF.

References

- ¹ B. T. Fedoroff, O. E. Sheffield, *Encyclopedia of Explosives and Related Items*, Picatinny Arsenal Dover, New Jersey, USA, 1962.
- ² T. M. Klapötke, *Energetic Materials Encyclopedia*, De Gruyter, Berlin, 2018.
- ³ P. Levy, S. Compton, R. Welch, G. Delgado, A. Jennett, N. Penugonda, R. Dunne, R. Zalenski, *Ann. Emerg. Med.*, 2007, **50**, 144-152.
- ⁴ W. R. Taylor, J. S. Forrester, P. Magnusson, T. Takano, K. Chatterjee, J. C. Swan, *Am. J. Cardiol.* 1976, **38**, 469-473.
- ⁵ A. Daiber, T. Münzel, *Advanced Protocols in Oxidative Stress II*, 2010, **594**, 311-326.
- ⁶ F. G. Shellock, P. K. Shah, D. S. Berman, S. A. Rubin, B. N. Singh, H. J. C. Swan, *Clin. Pharmacol. Ther.*, 1980, **28**, 436-440.
- ⁷ A. Daiber, T. Münzel, *Antioxid Redox Signal.*, 2015, **23**, 899-942.
- ⁸ W. L. Faust, *Science*, 1989, **245**, 37-42.
- ⁹ S. Zeman and M. Jungova, *Propellants Explos. Pyrotech.* 2016, **4**, 426-451.
- ¹⁰ W. Taylor, G. Morris, *Trans. Faraday Soc.*, 1971, **28**, 545-558.
- ¹¹ K. T. Lorenz, E. L. Lee, R. Chambers, *Propellants Explos. Pyrotech.*, 2015, **40**, 95-108.
- ¹² E. P. Wigner, *Science* 1948, **108**, 517-521.
- ¹³ L. L. Baxter, S. Huey, J. Lipkin, D. Shah, J. Ross, G. Sclipa, *Int. J. Energetic Materials Chem. Prop.*, 1997, **4**, 167-176.
- ¹⁴ C. A. Myler, W. M. Bradshaw, M. G. Cosmos, *J. Hazard. Mater.*, 1991, **26**, 333-342.
- ¹⁵ S. B. Kim, K. J. Kim, M. H. Cho, J. H. Kim, K. T. Kim, S. H. Kim, *ACS Appl. Mater. Interfaces*, 2016, **8**, 9405-9412.
- ¹⁶ R. Schlögl, *Angew. Chemie Int. Ed*, 2015, **54**, 3465-3520.
- ¹⁷ M. Pelaez, N. T. Nolan, S. C. Pillai, M. K. Seery, P. Falaras, A. G. Kontos, P. S.M. Dunlop, J. W.J. Hamilton, J. Byrne, K. O'Shea, M. H. Entezari, D. D. Dionysiou, *Applied Catalysis B*, 2012, **125**, 331-349.
- ¹⁸ M. Jing, R. Hong, W. Shao, H. Lin, D. Zhang, S. Zhuang, D. Zhang, *Optics Express* 2017, **25**, A1132.
- ¹⁹ M. Ratner, *Nature*, 1999, **397**, 480-481.
- ²⁰ J. S. Levine, C. P. Rinsland, G. M. Tennille, *Nature*, 1985, **318**, 254-257.
- ²¹ H. B. Singh, L. J. Salas, W. Viezee, *Nature*, 1986, **321**, 588-591.
- ²² L. A. Pinnaduwege, A. Gehl, D. L. Hedden, G. Muralidharan, T. Thundat, R. T. Lareau, T. Sulchek, L. Manning, B. Rogers, M. Jones, J. D. Adams, *Nature*, 2003, **425**, 474.
- ²³ A. Rose, Z. Zhu, C. F. Madigan, T. M. Swager, V. Bulovic, *Nature*, 2005, **434**, 876-879.

-
- ²⁴ T. L. Andrew, T. M. Swager, *J. Am. Chem. Soc.* 2007, **129**, 7254–7255.
- ²⁵ M. N. Germain, R. L. Arechederra, S. D. Minter, *J. Am. Chem. Soc.* 2008, **130**, 15272–15273.
- ²⁶ C. H. L. Go, W. H. Waddell, *J. Am. Chem. Soc.* 1984, **106**, 715–718.
- ²⁷ Z. Chen, S. Liu, M. Q. Yang, Y. J. Xu, *ACS Appl. Mater. Interfaces*, 2013, **5**, 4309–4319.
- ²⁸ E. Hrischlauff, R.G.W. Norrish, *J. Chem. Soc.*, 1936, **1**, 1580–1585.
- ²⁹ A. N. Frolov, N. A. Kuznetsova, A. V. El'tsov, *Russ. Chem. Rev.*, 1976, **45**, 1024–1034.
- ³⁰ E. D. Aluker, A. G. Krechetov, A. Y. Mitrofanov, Y. P. Sakharchuk, *Russ. J. Phys. Chem. B*, 2011, **5**, 821–823.
- ³¹ E. D. Aluker, A. G. Krechetov, A. Yu. Mitrofanov, D. R. Nurmukhametov, M. M. Kuklja, *J. Phys. Chem. C*, 2011, **115**, 6893–6901.
- ³² W. Zhang, X. Ma, R. Shen, L. Wu, Y. Ye, Y. Hu, P. Zhu, *Appl. Spectrosc. Rev.*, 2014, **49**, 550–563.
- ³³ E. R. Bernstein, *Energetic Mater.* 2014, **69**, 31–52.
- ³⁴ A.V. Akimov, A. J. Neukirch, O. V. Prezhdo, *Chem. Rev.*, 2013, **113**, 4496–4565.
- ³⁵ A. Migani, M. J. Bearpark, M. Olivucci, M. A. Robb, *J. Am. Chem. Soc.*, 2007, **129**, 3703–3713.
- ³⁶ M.M. Kuklja, *Applied Physics A-Materials Science and Processing*, 2003, **76** (3), 359–366.
- ³⁷ M.M. Kuklja, E.V. Stefanovich and A.B. Kunz, *J. of Chem. Physics*, 2000, **112**(7), 3417–3423.
- ³⁸ R. V. Tsyshevsky, S. N. Rashkeev, M. M. Kuklja, *Surf. Sci.*, 2015, **637–638**, 19–28.
- ³⁹ R.V. Tsyshevsky, A. Zverev, A. Mitrofanov, S. N. Rashkeev, M. M. Kuklja, *Molecules*, 2016, **21**, 289–1–13.
- ⁴⁰ P. Hohenberg, W. Kohn, *Phys. Rev. B*, 1964, **136**, 864–871.
- ⁴¹ W. Kohn and L. J. Sham, *Phys. Rev. A*, 1965, **140**, 1133–1138.
- ⁴² J. P. Perdew, K. Burke, M. Ernzerhof, *Phys. Rev. Lett.*, 1996, **77** 3865–3868.
- ⁴³ P. E. Blöchl, *Phys. Rev. B*, 1994, **50**, 17953–17979.
- ⁴⁴ G. Kresse and J. Furthmüller, *Comput. Mater. Sci.*, 1996, **6**, 15–50.
- ⁴⁵ G. Kresse and J. Furthmüller, *Phys. Rev. B*, 1996, **54**, 11169–86.
- ⁴⁶ G. Kresse and J. Hafner, *Phys. Rev. B*, 1993, **47**, 558–61.
- ⁴⁷ R. C. Whited and W. C. Walker, *Phys. Rev. Lett.*, 1969, **22**, 1428–1430.
- ⁴⁸ C. Adamo, V. Barone, *J. Chem. Phys.*, 1999, **110**, 6158–6169.
- ⁴⁹ M. Dion, H. Rydberg, E. Schroder, D. C. Langreth, B. I. Lundqvist, *Phys. Rev. Lett.*, 2004, **92**, 246401.
- ⁵⁰ J. Klimeš, D. R. Bowler, A. Michaelides, *J. Phys.: Cond. Matt.*, 2009, **22**, 022201–1–5.
- ⁵¹ J. Klimeš, D. R. Bowler, A. Michaelides, *Phys. Rev. B*, 2011, **83**, 195131.
- ⁵² G. Roman-Perez, J. M. Soler, *Phys. Rev. Lett.*, 2009, **103**, 096102.
- ⁵³ T. Thonhauser, V. R. Cooper, S. Li, A. Puzder, P. Hyldgaard, and D. C. Langreth, *Phys. Rev. B*, 2007, **76**, 125112.
- ⁵⁴ F. Neese, *WIREs Comput. Mol. Sci.*, 2012, **2**, 73–78.
- ⁵⁵ L. Giordano, G. Pacchioni, T. Bredow, J. F. Sanz, *Surf. Sci.*, 2001, **471**, 21–31
- ⁵⁶ A. D. Becke, *J. Chem. Phys.*, 1993, **98**, 5648–5652.
- ⁵⁷ C. Lee, W. Yang, R. G. Parr, *Phys. Rev. B*, 1988, **37**, 785–89.
- ⁵⁸ M. J. Frisch, G. W. Trucks, H. B. Schlegel, G. E. Scuseria, M. A. Robb, J. R. Cheeseman, G. Scalmani, V. Barone, B. Mennucci, G. A. Petersson, H. Nakatsuji, M. Caricato, X. Li, H. P. Hratchian, A. F. Izmaylov, J. Bloino, *et al.* Gaussian 09, revision B.01;Gaussian, Inc.: Wallingford, CT, 2010.
- ⁵⁹ R. Bauernschmitt and R. Ahlrichs, *Chem. Phys. Lett.*, 1996, **256**, 454–64.

-
- ⁶⁰ M. E. Casida, C. Jamorski, K. C. Casida, D. R. Salahub, *J. Chem. Phys.* **1998**, *108*, 4439-4449.
- ⁶¹ G. Pacchioni, *Surf. Rev. Lett.* **2000**, *7*, 277-306.
- ⁶² G. Spoto, E. N. Gribov, G. Ricchiardi, A. Damin, D. Scarano, S. Bordiga, A. Zecchina, *Prog. Surf. Sci.*, 2004, **76**, 71-146.
- ⁶³ P. V. Sushko, A. L. Shluger, C. Richard, A. Catlow, *Surf. Sci.*, 2000, **450**, 153-170.
- ⁶⁴ P. V. Sushko, J. L. Gavartin, A. L. Shluger, *J. Phys. Chem. B*, 2002, **106**, 2269-2276.
- ⁶⁵ W. P. Hess, A. G. Joly, K. M. Beck, M. Henyk, *J. Phys. Chem. B*, 2005, **109**, 19563-19578.
- ⁶⁶ K. P. McKenna, P. V. Sushko, A. L. Shluger, *J. Am. Chem. Soc.*, 2007, **129**, 8600-8608.
- ⁶⁷ G. Pacchioni, S. Siculo, C. Di Valentin, M. Chiesa, E. Giamello, *J. Am. Chem. Soc.*, 2008, **130**, 8690-8695.
- ⁶⁸ M. Sterrer, E. Fischbach, T. Risse, H. J. Freund, *Phys. Rev. Lett.*, 2005, **94**, 186101.
- ⁶⁹ K. M. Neyman, C. Inntam, A. V. Matveev, V. A. Nasluzov, N. Rösch, *J. Am. Chem. Soc.*, 2005, **127**, 11652-11660.
- ⁷⁰ Z. Yan, S. Chinta, A. A. Mohamed, J. P. Fackler, D. W. Goodman, *J. Am. Chem. Soc.*, 2005, **127**, 1604-1605.
- ⁷¹ M. Roessler, and W. C. Walker, *Phys. Rev.*, 1967, **159**, 733-738.
- ⁷² P. A. Cox, A. A. Williams, *Surf. Sci. Lett.*, 1986, **175**, L782-L786.
- ⁷³ R.V. Tsyshevsky, O. Sharia, M.M. Kuklja, *J. Phys. Chem. C*, 2014, **118**, 9324-9335.
- ⁷⁴ P. A. Mullen, M. K. Orloff, *J. Phys. Chem.*, 1973, **77**, 910-911.
- ⁷⁵ Z. Yu, E. R. Bernstein, *J. Chem. Phys.*, 2011, **135**, 154305-154305-10.
- ⁷⁶ J. K. Cooper, C. D. Grant, J. Z. Zhang, *J. Phys. Chem. A*, 2013, **117**, 6043-6051.
- ⁷⁷ R.V. Tsyshevsky, O. Sharia, M. M. Kuklja, *J. Phys. Chem. C*, 2014, **118**, 26530-26542.
- ⁷⁸ J. C. Oxley, J. L. Smith, J. E. Brady IV, A. C. Brown, *Propellants Explos. Pyrotech.*, 2012, **37**, 24-39.
- ⁷⁹ R. V. Tsyshevsky, O. Sharia, M. M. Kuklja, *J. Phys. Chem. C*, 2013, **117**, 18144-18153
- ⁸⁰ R. Cohen, Y. Zeiri, E. Wurzburg, R. Kosloff, *J. Phys. Chem. A*, 2007, **111**, 11074-11083.
- ⁸¹ B. Nguyen Van, E.V. Nikolaeva, A.G. Shamov, G.M. Khrapkovskii, R.V. Tsyshevsky, *Int. J. Mass Spectrometry*, 2015, **392**, 7-15.
- ⁸² D. L. Paisley, *Proceedings 9th Symposium (International) on Detonation*, 1989, 1110-1117.
- ⁸³ R. Akhmetshin, A. Razin, V. Ovchinnikov, A. Skripin, V. Tsipilev, V. Oleshko, V. Zarko, A. Yakovlev, *J. Phys.: Conf. Ser.* 2014, **552**, 012015
- ⁸⁴ M.M.Kuklja, *Advances in Quantum Chemistry: Energetic Materials*, 2014, **68**, edited by John R. Sabin and Erkki Brändas, Elsevier Inc., pp. 71-146.
- ⁸⁵ E. D. Aluker, A. G. Krechetov, A. Y. Mitrofanov, A. S. Zverev, and M. M. Kuklja, *Molecules* 2013, **18**, 14148-14160.